Ozone response to precursor controls in very complex terrains: Use of photochemical indicators to assess O_3-NO_x-VOC sensitivity in the northeastern Iberian Peninsula

Pedro Jiménez and José M. Baldasano

Laboratory of Environmental Modeling, Universitat Politècnica de Catalunya (UPC), Barcelona, Spain

Received 4 May 2004; revised 18 June 2004; accepted 12 July 2004; published 30 October 2004.

[1] The kinetics of ozone (O_3) chemistry and its two main precursors, nitrogen oxides (NO_x) and volatile organic compounds (VOC), represents an important field of uncertainty in atmospheric chemistry and photochemical modeling. This uncertainty affects the design of control strategies to reduce tropospheric O_3 production. The effect of controlling ozone precursors on sensitivity regimes was evaluated by performing simulations with MM5-EMICAT2000-CMAQ model to represent O_3 formation in the northeastern Iberian Peninsula with baseline emission rates for VOC and NO_x, and reducing anthropogenic VOC and NO_x emissions on a 35%. Three different scenarios were considered in order to assess chemical sensitivity in urban, industrial, and background domains. Areas downwind of the city of Barcelona benefit from NO_x reductions (reduction of 10 ppb in ground-level O_3), while the same reduction causes an important increment of O_3 in Barcelona (9 ppb) and the area downwind of Tarragona (18 ppb), with a high industrial influence. The city of Barcelona benefits from VOC reductions (10 ppb of O_3) as well as the industrial zone of Alcover (20 ppb). The rest of the domain is practically insensitive to VOC reductions. Diverse photochemical species derived from the air quality model were used as indicators in order to establish the chemical sensitivity regime existing in the areas, analyzing whether O_3 values reacted consistently to similar changes in emissions. Results showed that NO_y (total reactive nitrogen) and O_3/NO_y are the indicators involving a lower uncertainty when assessing sensitivity, according to the narrow transition regime between NO_x- and VOC-sensitive chemistry and the low uncertainty observed. Indicators performed better in VOC-sensitive than in NO_x-sensitive domains. H_2O_2- and HNO_3- derived indicators entailed higher uncertainties since transition regimes between NO_x and VOC sensitivity covered a wide range. The extent of reaction also performed as a good indicator to separate NO_x- and VOC-sensitive regimes. This sensitivity analysis provides a tool for establishing hypothetical control policies for O_3 precursor emissions through a comparison of simulated correlation between the species. *INDEX TERMS:* 0345 Atmospheric Composition and Structure: Pollution—urban and regional (0305); 0368 Atmospheric Composition and Structure: Troposphere—constituent transport and chemistry; 0365 Atmospheric Composition and Structure: Troposphere—composition and chemistry; 3210 Mathematical Geophysics: Modeling; *KEYWORDS:* air quality modeling, tropospheric ozone, precursor controls, model evaluation

Citation: Jiménez, P., and J. M. Baldasano (2004), Ozone response to precursor controls in very complex terrains: Use of photochemical indicators to assess O_3-NO_x-VOC sensitivity in the northeastern Iberian Peninsula, *J. Geophys. Res.*, *109*, D20309, doi:10.1029/2004JD004985.

1. Introduction

[2] The kinetics of ozone (O_3) chemistry and its two main precursors, nitrogen oxides (NO_x) and volatile organic compounds (VOC) represents an important field of uncertainty in atmospheric chemistry and photochemical modeling [*Atkinson*, 2000]. It is generally known that under some conditions, O_3 concentrations increase with increasing NO_x and are largely insensitive to VOC, while for other conditions the rate of formation will increase with increasing VOC and will be unchanged or decrease with increasing NO_x. This complexity affects the design of control strategies to reduce tropospheric O_3 production, and considerable interest exists in finding observable indicators of how real air masses are likely to respond to emission controls.

[3] A major problem for the study of O_3-NO_x-VOC sensitivity has been the inability to gain evidence based on direct measurements rather than theoretical calculations [*Sillman*, 1999]. This problem has been especially critical

0148-0227/04/2004JD004985$09.00

when different models have given contradictory results on the effectiveness of NO_x versus VOC control.

[4] *Milford et al.* [1994] developed an approach for evaluating NO_x-VOC sensitivity. They found that model predictions for NO_x-VOC sensitivity were linked to simulated concentrations of a number of key species. VOC-sensitive ozone in models is associated with afternoon values of total reactive nitrogen (NO_y) above a certain threshold concentration, while NO_x sensitivity ozone was associated with lower NO_y. *Sillman* [1995] and *Sillman et al.* [1998] extended the work of *Milford et al.* [1994] in order to include other indicator species and ratios: O_3/NO_y, O_3/NO_z (where NO_z is defined as NO_y-NO_x), and H_2O_2/HNO_3. In recent years, a number of works have deepened in the analysis of photochemical indicators that determine the split into VOC-sensitive and NO_x-sensitive regimes [*Tonnesen and Dennis*, 2000a, 2000b; *Blanchard and Stoeckenius*, 2001; *Blanchard and Fairley*, 2001; *Sillman and He*, 2002; *Sillman et al.*, 2003]. Nevertheless, it is still unclear whether the indicator ratios would show similar behavior for a wide variety of conditions.

[5] *Blanchard et al.* [1999] and *Blanchard and Stoeckenius* [2001] used the extent of reaction parameter (EOR) to describe how far a system has proceeded toward its maximum possible O_3 production, with the transition from radical to NO_x limitation typically occurring when the extent of reaction is 0.9 (dimensionless units). EOR was derived from smog chamber experiments and is based on the finding that O_3 in photochemically aged air is sensitive to NO_x while air with relatively unprocessed emissions is sensitive to VOC. Box model and three-dimensional model simulations indicate that when the extent of reaction remains below ~0.6 during the hours of peak ozone, O_3 formation is limited by the availability of radicals, rather than NO_x, and O_3 concentrations respond to changes in VOC levels [*Blanchard and Fairley*, 2001].

[6] Here we show results from model calculations that relate NO_x-VOC sensitivity in as very complex an area as the northeastern Iberian Peninsula. We use a three-dimensional air quality model (MM5-EMICAT2000-CMAQ) to represent O_3 formation and transport. A series of scenarios are analyzed in order to establish their chemical regime. Using the model to study three different scenarios gives the opportunity to compare the variation of indicator values in each zone and to check whether O_3 values react consistently to similar changes in emissions. Correlations between model species concentrations and NO_x-VOC sensitivity predictions are examined to see whether commonly employed indicators can be correlated with NO_x-VOC sensitivity in the case of northeastern Iberian Peninsula. This O_3 sensitivity analysis provides an evaluation of NO_x and VOC hypothetical control policies through a comparison of simulated correlation between the species.

2. Use of Indicator Species

[7] The split between NO_x-sensitive and VOC-sensitive conditions is well known. For conditions with relatively high VOC and low NO_x, O_3 increases with increasing NO_x and is relatively insensitive to changes in VOC. For conditions with relatively low VOC and high NO_x, O_3 increases with increasing VOC and decreases with increasing NO_x. An analogous split between "NO_x-sensitive" and "NO_x-saturated" regimes occurs in the remote troposphere, although for remote conditions O_3 increases with increasing VOC even in the NO_x-sensitive regime [*Sillman and He*, 2002]. These phenomena are driven by the complex ozone chemistry.

[8] The split between NO_x-sensitive and VOC-sensitive regimes is driven by the chemistry of odd hydrogen radicals. The NO_x-VOC split is attributed to the relative rate of formation of peroxides (via HO_2-HO_2 and HO_2-RO_2 reactions) relative to nitric acid formation (via reaction OH + NO_2). NO_x-sensitive conditions occur when peroxides dominate over nitric acid as radical sinks, while NO_x-saturated conditions occur when nitric acid dominates [*Sillman*, 1999]. NO_x-VOC sensitivity is attributed to the relative source strengths of odd hydrogen radicals (S_H) and odd nitrogen (S_N), summed over the period of O_3 production for an air parcel [*Sillman and He*, 2002]. VOC-sensitive chemistry occurs when the odd nitrogen source exceeds the source of odd hydrogen. According to *Kleinman et al.* [1997], the instantaneous rate of O_3 production is VOC-sensitive whenever the instantaneous loss rate for odd nitrogen (L_N) is greater then half of the total odd hydrogen source ($L_N/Q > 0.5$). Odd hydrogen sources must be in steady state with its three major sinks (equation (1)):

$$S_H = 2P_{perox} + P_{HNO3} + P_{PANS} \quad (1)$$

where P_{perox} and P_{HNO3} represent production rates for peroxides (including H_2O_2 and organic peroxides) and HNO_3, and P_{PANS} represents net photochemical production of peroxyacetyl nitrate (PAN) and higher-order analogues. VOC-sensitive chemistry would occur whenever P_{HNO3} exceeds $2P_{perox}$. The NO_x-VOC split is mainly associated with formation of nitric acid but is not greatly affected by formation of PAN. Sensitivity transition from NO_x-sensitive to VOC-sensitive conditions can be defined in equation (2) [*Sillman and He*, 2002]:

$$\frac{1}{Q_N}\frac{\partial[O_3]}{\partial Q_N} = \frac{1}{Q_H}\frac{\partial[O_3]}{\partial Q_H} \quad (2)$$

where $[O_3]$ represents ozone concentrations and Q_N and Q_H represent emission rates for NO_x and VOC. Using this definition, the sensitivity transition represents the point at which a given percent reduction in either NO_x or VOC would result in the same reduction in ozone.

[9] *Tonnesen and Dennis* [2000a] analyzed O_3 formation in terms of radical formation equivalent, radical termination (through production of peroxides, HNO_3 and organic nitrates) and radical propagation, finding out that production rate for O_3 is proportional to the rate of the VOC + OH reactions. *Sillman* [1995] suggested that O_3 was roughly proportional to the odd hydrogen source, being the ratio O_3/NO_z analogous to the quotient S_H/L_N, which is related to NO_x-VOC sensitivity. Following this basis, *Sillman* [1995] proposed some indicators including O_3/NO_y, O_3/NO_z, O_3/HNO_3, H_2O_2/HNO_3, H_2O_2/NO_z and

the equivalent ratios with summed H_2O_2 and organic peroxides.

3. Methodology

[10] Modeling results are based on a photochemical pollution event in the Western Mediterranean Basin that took place on 13–16 August 2000. Simulation shows the results for 14 August 2000, which is a representative day of this episode, and values around the European threshold of 90 ppb for tropospheric O_3 are attained. The domain of study (Figure 1) covers a squared area of 272 × 272 km^2 centered in Catalonia, located in the northeastern Iberian Peninsula. The complex configuration of the zone is influenced by the presence of the Pyrenees mountain range (with altitudes over 3000 m), the large valley canalization of Ebro river and the Mediterranean Sea. That produces a sharp gradient in the characteristics of the northeastern Iberian Peninsula. The effect of controlling ozone precursors on sensitivity regimes was evaluated performing simulations for the domain with baseline emission rates for VOC and NO_x as derived from EMICAT2000 model, and reducing anthropogenic VOC and NO_x emissions on a 35% following the methods by *Milford et al.* [1994], *Sillman* [1995], and *Sillman et al.* [2003]. Meteorology represents the same day in order not to introduce any external influence. Three inner scenarios were deeply analyzed at 1200 UTC, the hour of maximum ground-level O_3 production: (1) a 32 × 32 km^2 urban area centered in the city of Barcelona that comprises the Barcelona geographical area (BGA); (2) a 32 × 32 km^2 background area centered in Plana de Vic (VIC); and (3) a 32 × 32 km^2 industrial zone centered in Alcover (ALC). The selection of these scenarios is based in the important photochemical pollution episodes in the northeastern Iberian Peninsula.

3.1. Models

[11] MM5 numerical weather prediction model [*Mesoscale and Microscale Meteorology Division*, 2001] provided the meteorology dynamical parameters. MM5 physical options used for the simulations were: Mellor-Yamada scheme as used in the Eta model for the PBL parameterization; Anthes-Kuo and Kain-Fritsch cumulus scheme; Dudhia simple ice moisture scheme, the cloud radiation scheme, and the five-layer soil model. Initialization and boundary conditions for the mesoscale model were introduced with analysis data of the European Center of Medium-range Weather Forecasts global model (ECMWF). Data were available at a 1° resolution (100 km approximately at the working latitude) at the standard pressure levels every 6 hours.

[12] The high-resolution (1 h and 1 km^2) EMICAT2000 emission model has been applied in the northeastern Iberian Peninsula. As precursors of photochemical smog, the model estimates the cell emissions of nitrogen oxides (NO_x), nonmethane volatile organic compounds (NMVOCs), carbon monoxide (CO), and also total suspended particles (TSP) and sulphur dioxide (SO_2). This emission model includes the emissions from vegetation, on-road traffic, industries and emissions by fossil fuel consumption and domestic-commercial solvent use. Biogenic VOC (BVOC) emissions were estimated using a methodology that takes into account local vegetation data (land use distribution and biomass factors) and meteorological conditions (surface air temperature and solar radiation) together with emission factors for native Mediterranean species and cultures [*Parra et al.*, 2004]. On-road traffic emission includes the hot exhaust, cold exhaust and evaporative emissions using the methodology and emission factors of the European model EMEP/CORINAIR – COPERTIII [*Ntziachristos and Samaras*, 2000] as basis, and differencing the vehicle park composition between weekdays and weekends [*Parra and Baldasano*, 2004]. Industrial emissions include real records of some chimneys connected to the emission control net of the Department of the Environment of Catalonia, and the estimated emissions from power stations (conventional and cogeneration units), incinerators, cement factories, refineries, olefins plants and chemical industries.

[13] The chemical transport model used to compute the concentrations of photochemical pollutants was Models-3/CMAQ [*Byun and Ching*, 1999]. The initial and boundary conditions were derived from a one-way nested simulation covering a domain of 1392 × 1104 km^2 centered in the Iberian Peninsula through a 48-hour spin-up. The chemical mechanism selected for simulations was CBM-IV [*Gery et al.*, 1989], including aerosols and heterogeneous chemistry. The algorithm chosen for the resolution of tropospheric chemistry was the Modified Euler Backward Iterative (MEBI) method [*Huang and Chang*, 2001]. Horizontal resolution considered was 2 km, and 16-sigma vertical layers cover the troposphere.

3.2. Scenarios

[14] The synoptic situation of 14 August 2000 corresponds to a typical summertime low pressure gradient over the Iberian Peninsula. The day was characterized by a weak synoptic forcing, so that mesoscale phenomena, induced by the particular geography of the region would be dominant. This situation is associated with weak winds in the lower troposphere and high maximum temperatures. A high sea level pressure and almost nonexistent surface pressure gradients over the domain characterize this day, with slow northwesterlies aloft. Under this weak synoptic forcing, strong insolation promotes the development of prevailing mesoscale flows associated with the local orography (mountain and valley breezes), while the difference of temperature between the sea and the land enhances the development of sea-land breezes [*Barros et al.*, 2003]. *Millán et al.* [1997] generally described the recirculations processes occurring along the Western Mediterranean Basin under this synoptic situation. During the day the sea breezes transport coastal pollutants inland, while at the leading edge of the breeze front breezes combine with upslope winds to inject a large fraction of these pollutants in return flows aloft at heights ranging from 2 to 3 km. Once in those upper layers, pollutants move back toward the sea [*Baldasano et al.*, 1994], the air at the middle troposphere is forced to go down by the subsidence over the east coast, once in low levels the air masses recirculate over the sea with a possible later return to the seaboard later. *Pérez et al.* [2004] confirmed this behavior when analyzing the characteristic recircula-

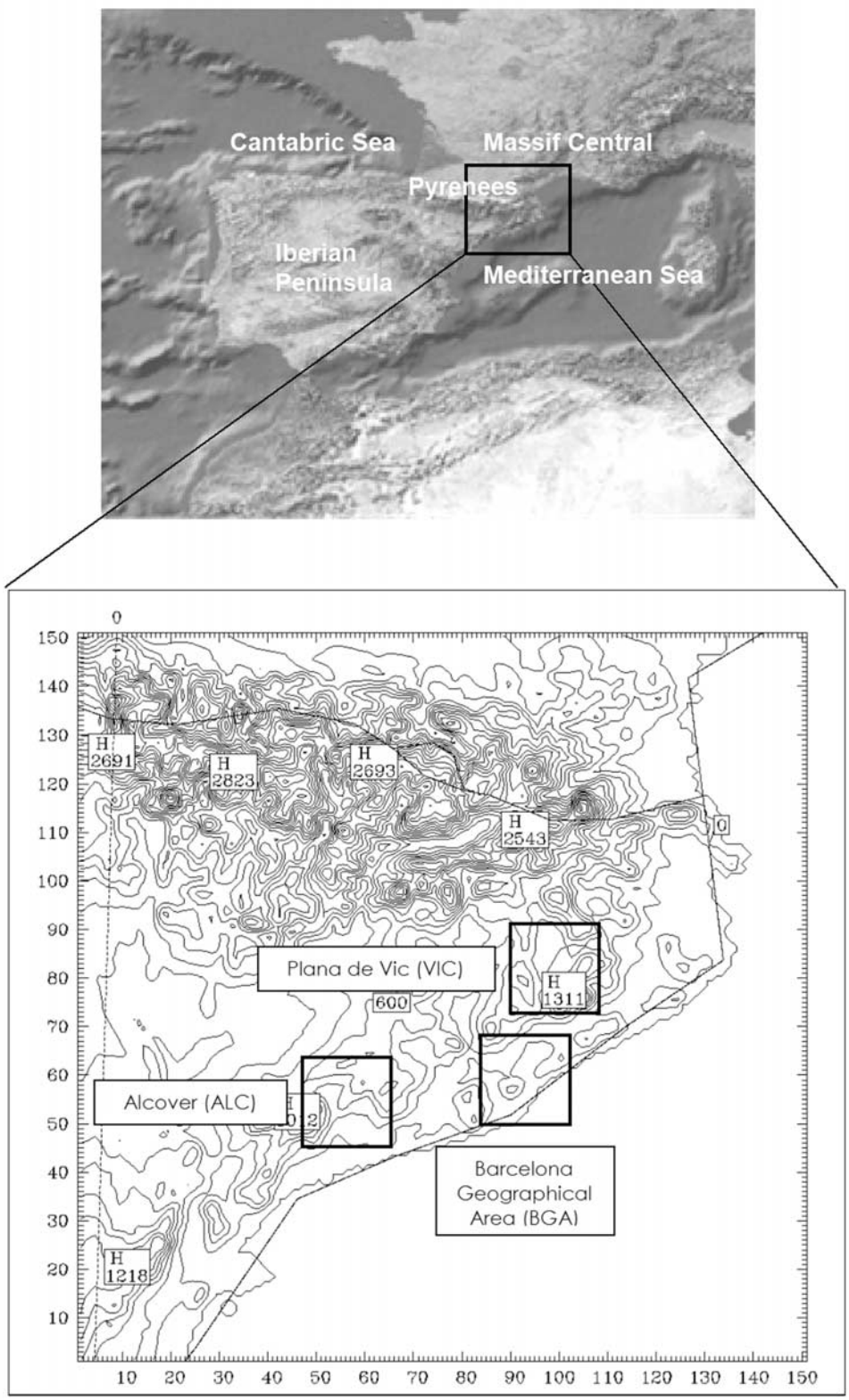

Figure 1. Location and orography of the three domains under study: Barcelona geographical area (BGA, urban), Plana de Vic (VIC, background) and Alcover (ALC, industrial).

tions produced along the east coast of the Iberian Peninsula for 14 August 2000. This situation is representative of an episode of photochemical pollution in the Western Mediterranean Basin, since the occurrence of regional recirculations at low levels represents 45% of the yearly flow transport patterns over the area of study [*Jorba et al.*, 2004] and these situations are associated with local regional episodes of air pollution in the northeastern

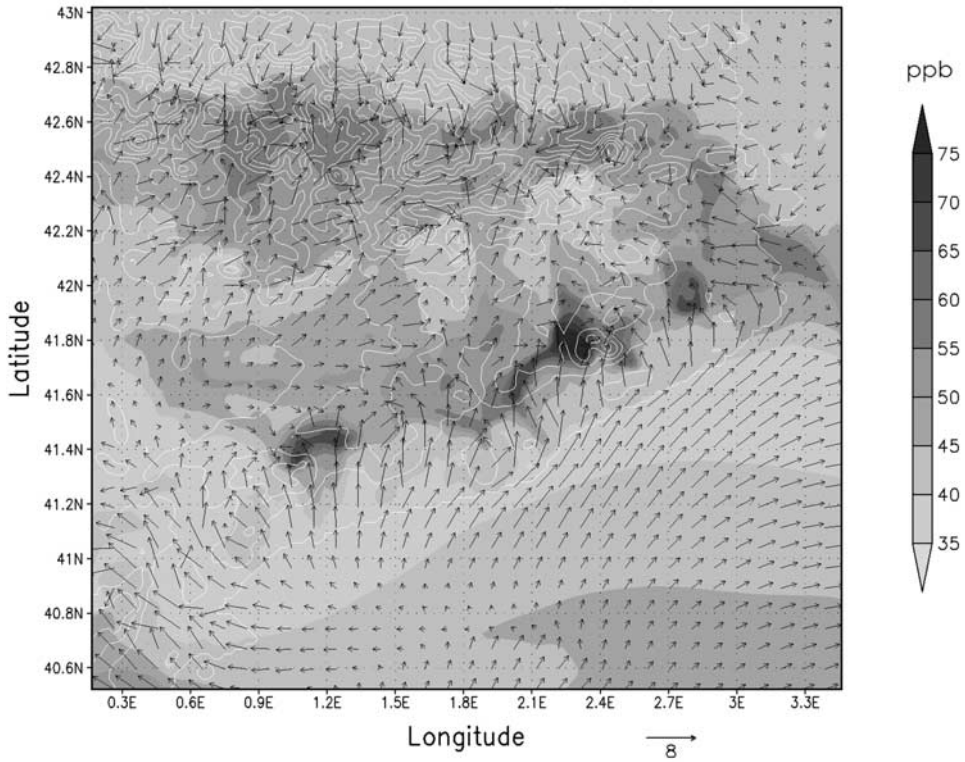

Figure 2. Surface ozone concentration and wind fields at 1200 UTC on 14 August 2000 in the northeastern Iberian Peninsula, as simulated by MM5-EMICAT2000-CMAQ air quality model.

Iberian Peninsula that result in high levels of ozone and an increase of particulate matter within the boundary layer during summer [*Toll and Baldasano*, 2000; *Barros et al.*, 2003].

[15] The main emissions sources in the northeastern Iberian Peninsula are located on the coast [*Parra*, 2004]. Total emissions of ozone precursors during 14 August 2000 were 236 t d^{-1} for NO_x and 172 t d^{-1} for VOCs. Importance of biogenic emissions is high in the area, since this source represents 34% of VOCs emissions in the northeastern Iberian Peninsula during this summer episode and is an important source of reactive compounds such as aldehydes and isoprene. Road traffic accounts for a 58% of NO_x emissions and 36% of VOCs in the domain, specially olefins and aromatic compounds. Most important emitters are found along the road axis parallel to the coast and BGA. Industrial emissions are principally located in the industrial area of Alcover (ALC) and represent 39% of NO_x emissions and 17% of VOCs, meanwhile the use of residential and domestic solvent use provides the 13% of VOCs emissions in the area [*Parra*, 2004].

[16] The peculiar topography of the zone is the principal driving mechanism that contributes to the dispersion of emissions in the given domain. Maximum O_3 levels in Catalonia are measured in Plana de Vic and Alcover industrial zone (over 80 ppb). As derived from simulations (Figure 2), air masses from Barcelona Geographical Area are advected to the zone of Plana de Vic through river valley canalizations, transporting ozone precursors. These air masses departing from Barcelona act as photochemical reactors as they move northeast (the component of the wind is south-southwest) until they reach the region of Vic. Alcover high O_3 levels have a local origin according to the high weight of heavy chemical industry in the area.

3.3. Model-Measurement Comparisons

[17] Hourly measures of ground-level O_3 simulation results in each case and scenario were compared with the measurements from 48 air quality surface stations in northeastern Spain (Catalonia), which belong to the Environmental Department of the Catalonia Government and are located within the above scenarios. The nonavailability of measurements of other pollutants with an interest as indicators (e.g., NO_y, H_2O_2 or HNO_3) lead us to focus on the evaluation of ground-level O_3. The analysis of the results will consist of a statistical evaluation, comparing the first-layer simulations results and the values measured in the air quality stations of the domain under study. Meteorological model has also been evaluated comparing model results with surface and aloft wind measurements. Validation data of 52 surface stations located across the domain, and a radiosonde launched in Barcelona (in the center of the domain in the coast) were used.

[18] The U.S. Environmental Protection Agency (U.S. EPA) has developed guidelines [*U.S. EPA*, 1991] for a minimum set of statistical measures to be used for these evaluations where monitoring data are sufficiently dense. Those statistical figures are considered here are the mean normalized bias error (MNBE), the mean normalized gross error for concentrations above a prescribed threshold (MNGE), and the unpaired peak prediction accuracy (UPA). Observation-prediction pairs are often excluded from the analysis if the observed concentration is below a certain cutoff; the cutoff levels vary from study to study but

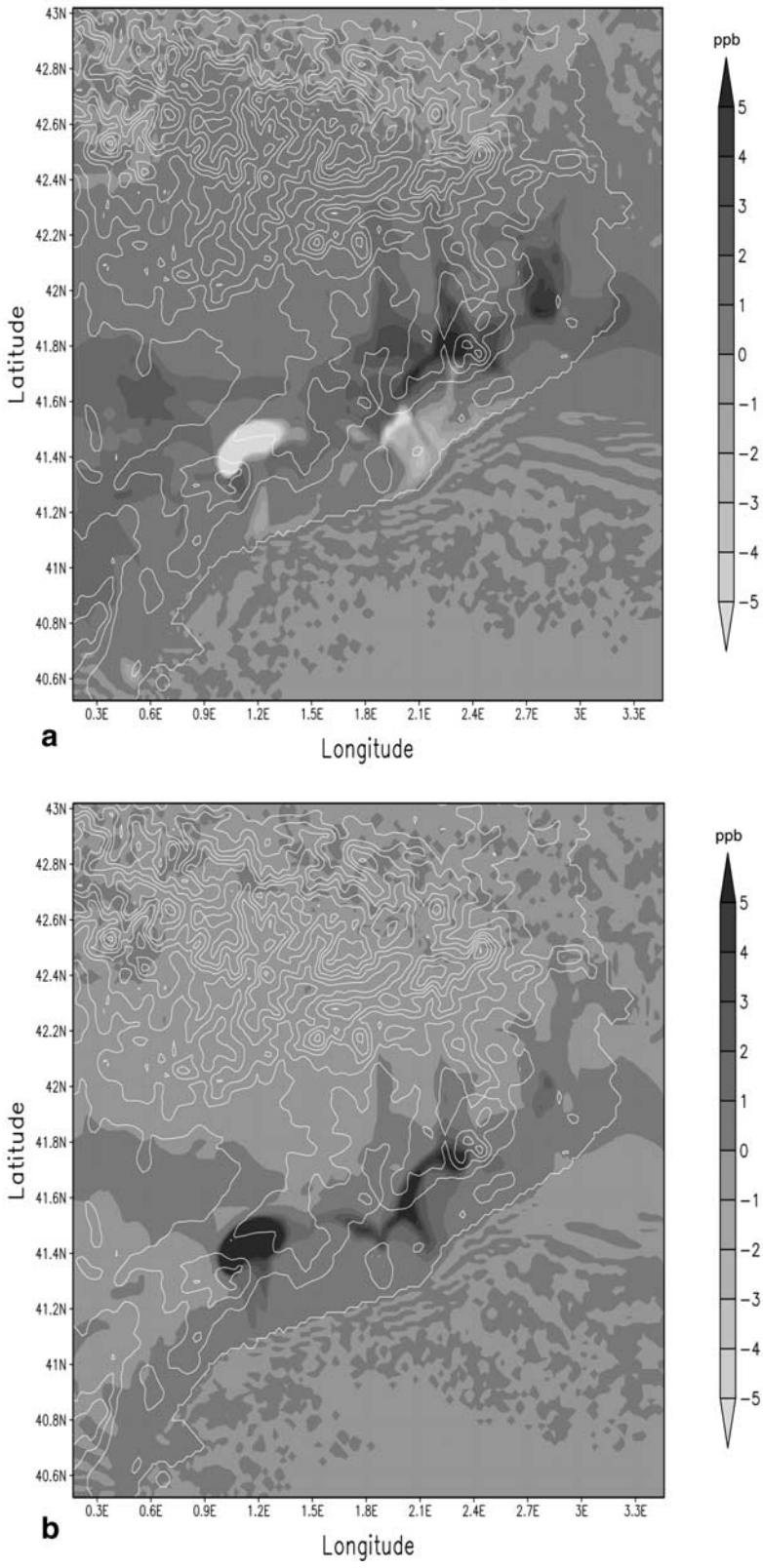

Figure 3. (a) Reduction in peak ozone concentrations (ppb) at 1200 UTC due to 35% reduction in NO_x emissions (base case−NO_x reduction case). Positive values imply O_3 reductions respect to the base case. Differences over 2 ppb indicate NO_x- or VOC- sensitive regimes. (b) Reduction in peak ozone concentrations (ppb) at 1200 UTC due to 35% reduction in VOC emissions (base case−VOC reduction case). Positive values imply O_3 reductions respect to the base case. Differences over 2 ppb indicate NO_x- or VOC- sensitive regimes. (c) Reduction in peak ozone concentrations (ppb) at 1200 UTC due to difference between VOC reduction case and NO_x reduction case.

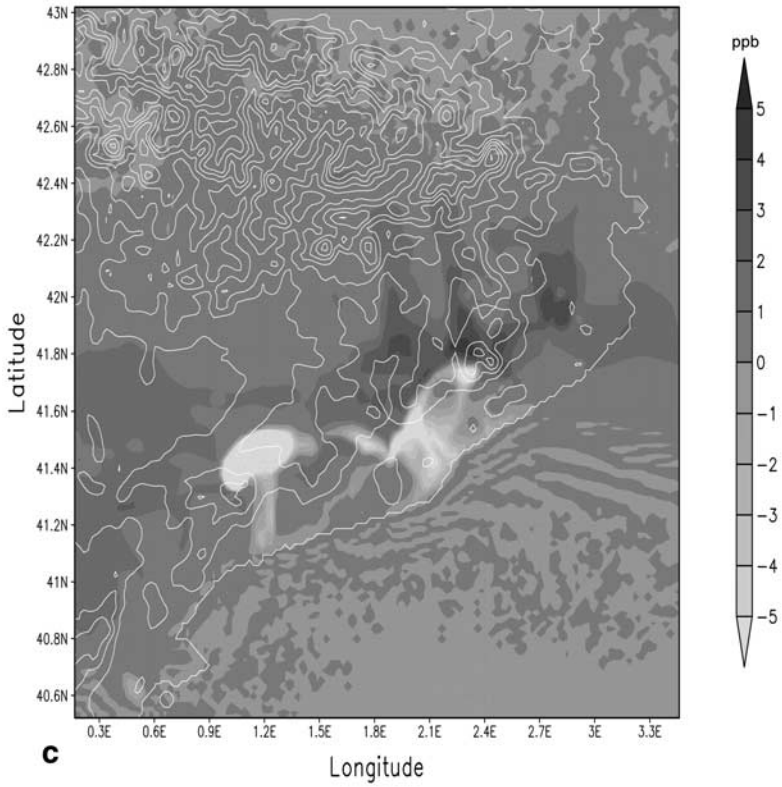

Figure 3. (continued)

often a level of 60 ppb is used [*Hogrefe et al.*, 2001], which is the criterion applied in this work.

4. Response to NO_x and VOC Controls

[19] The correspondence between NO_x-VOC sensitivity and indicator values can be examined in greater detail if quantitative methods are used to define NO_x-VOC chemistry. For these purposes, we could use the definition by *Sillman et al.* [2003]. Locations are defined as NO_x-sensitive for a specified hour if O_3 in the case with 35% reduced NO_x is lower than O_3 in both the base case and in the case with 35% reduced VOC by at least 2 ppb. Locations are classified as VOC-sensitive if the O_3 in the case with reduced VOC is lower than O_3 in the other cases by at least 2 ppb. Locations that are neither VOC-sensitive of NO_x-sensitive by this definition are classified as having mixed sensitivity if O_3 in the cases with the reduced NO_x and with reduced VOC is lower than O_3 in the base case by at least 2 ppb; locations are classified as insensitive to NO_x and VOC otherwise. These definitions are time-dependent; that is, a model location may be NO_x-sensitive at some times and VOC-sensitive at other times. *Lu and Chang* [1998] used another definition, which separates extreme cases, that is, locations where only NO_x or only VOC controls are effective. Their definition is based on zero lines of simulated reduction in peak O_3 associated with reduced NO_x, versus reduction associated with reduced VOC [*Andreani-Aksoyoglu et al.*, 2001].

[20] A preliminary examination of geographic patterns of responses to emission reductions at 1200 UTC shows that the area with the most elevated O_3 concentration (VIC), benefits from NO_x reductions (reduction of 10 ppb in ground-level O_3 levels), meanwhile the same reduction emissions causes an important increment of O_3 in the city of Barcelona (9 ppb) and downwind the industrial area of Tarragona (18 ppb) (Figure 3a). Cities located in BGA and the plume departing from the city of Barcelona benefit form VOC reductions (10 ppb of O_3), as well as the industrial zone of ALC (20 ppb) (Figure 3b). The rest of the domain is practically insensitive to VOC reductions. This behavior is more clearly seen when studying differences between O_3 levels in the case of 35% VOC reduction and 35% NO_x reduction (Figure 3c).

[21] Figure 4a illustrates the distribution of the cells of the domain according to their NO_x or VOC sensitivity using *Sillman et al.*'s [2003] definition, derived from BGA, VIC and ALC scenarios. This definition indicates locations where NO_x or VOC controls are more effective in reducing O_3 production. As derived from this definition, most cells in BGA and ALC are under a VOC-sensitive regime or have a mixed sensitivity; meanwhile VIC is dominated by a NO_x-sensitive chemistry.

[22] According to the criterion of *Lu and Chang* [1998], the grid cells in the top left quadrant of Figure 4b are characterized with NO_x-sensitive chemistry. They show considerable O_3 decrease with decreasing NO_x, and insignificant O_3 reduction when reducing VOC. This approach assumes that the grid cells in the top right quadrant are sensitive to both VOC and NO_x controls. Grid cells in the bottom right quadrant, where O_3 diminishes with decreasing VOC but increases with decreasing NO_x, are referred to as VOC sensitive grid cells. The bottom left quadrant is empty. According to this definition, most of the grid cells in BGA

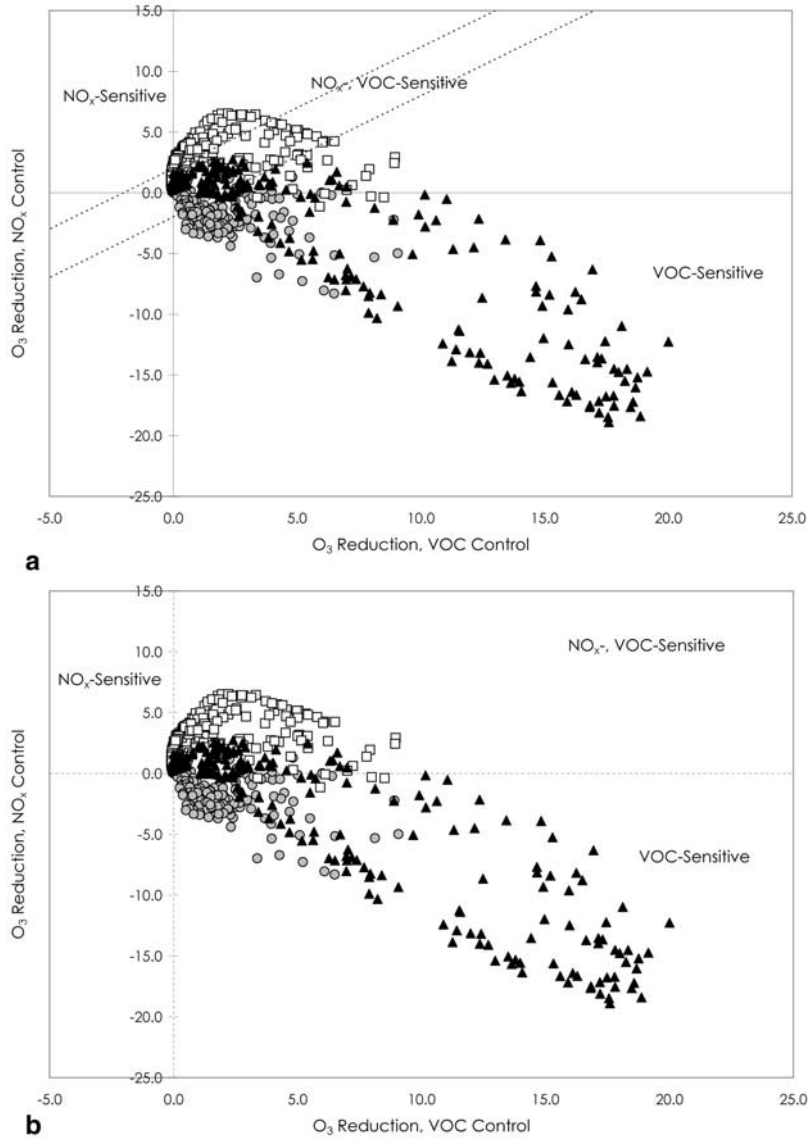

Figure 4. (a) Relation between ozone reductions due to NO_x controls (35% emission reduction) and VOC controls (35% emission reduction) for Barcelona geographical area (circles), Plana de Vic (squares), and Alcover (triangles) using the definition of *Sillman et al.* [2003]. (b) Relation between ozone reductions due to NO_x controls (35% emission reduction) and VOC controls (35% emission reduction) for Barcelona Geographical Area (circles), Plana de Vic (squares) and Alcover (triangles) using the definition of *Lu and Chang* [1998].

are VOC-sensitive, meanwhile cells in VIC have a mixed sensitivity. The domain of ALC is NO_x- and VOC-sensitive for several cells, meanwhile most of the domain presents a VOC-limited regime.

4.1. Model-Measurement Comparisons

[23] Despite that a surface measurement represents a value only at a given horizontal location and height, while the concentration predicted by the model represents a volume-averaged value, comparisons of model and measured variables represents a useful tool to depict the behavior of every case in the scenarios considered. Table 1 shows the root mean square error (RMSE) of wind speed at 10 m, for the lower, middle and upper troposphere and RMSE of wind direction (10 m) at 0000, 1200 and 2400 UTC. The general behavior of the model shows a tendency to overestimate nocturnal surface winds and to underestimate the diurnal flow. A clear improvement is produced in the simulation during the central part of the day; at this time, the complex structure of the sea breeze described by simulation and the development of up-slope winds appears to agree in a higher grade with surface measurements. The statistics show how the model presents a better behavior within the boundary layer, and major disagreement with the radiosonde appears over 1000 m above ground level.

[24] Although there is no objective criterion set forth for a satisfactory model performance in the case of ozone, suggested values of ±10–15% for MNBE, ±15–20% for

Table 1. RMSE Statistic of Wind Speed, and Wind Direction at 0000, 1200, and 2400 UTC for 14 August 2000[a]

	0000 UTC	1200 UTC	2400 UTC
RMSE wind speed, m/s			
Surface 10 m	1.71	2.04	2.00
Radio. <1000 m	0.84	1.04	1.31
1000–5000 m	5.03	1.55	3.7
5000–10000 m	8.45	5.15	3.94
RMSE wind direction, deg			
Surface 10 m	95.95	44.74	89.40

[a]Surface values were evaluated with 52 surface stations; aloft values were evaluated with a radiosonde.

the UPA and ±30–35% for the MNGE to be met by modeling simulations of O_3 have been considered for regulatory applications [*Russell and Dennis*, 2000; *Hogrefe et al.*, 2001]. Figure 5 and Table 2 show the results of the evaluation of ground-level O_3. Peak O_3 in the different scenarios is slightly lower than the measured values for each considered case. Comparison between model and measurements shows a good agreement when the model predicts dominant VOC-sensitive chemistry in the BGA and ALC scenarios. Here, statistical parameters of O_3 evaluation get worse when reducing VOC emissions and improve in the −35% NO_x case, specially in the Barcelona Geographical Area, where UPA reduces from −18% in the VOC reduction case until −8% in the NO_x reduction case). The same behavior is observed in Alcover. By contrast, the evaluation in VIC depicts a clear underprediction of O_3 levels (around −18% of MNBE, 27% of MNGE and −13% of UPA). Statistic parameters in the stations of Plana de Vic worsen when reducing precursor emissions on a 35%, especially in the case of 35% NO_x reduction, which yields to a more important underestimation of O_3 levels in the area because of the NO_x-limited regime of this scenario. It is noteworthy that all model cases meet the criteria established by U.S. EPA for model evaluations in the case of O_3.

[25] Model-measurement comparison suggests that the O_3 production chemistry may not be sufficiently reactive, possibly because of an underestimation in reactive VOC and/or an overestimation in NO_x emissions. The inferior bias compared to the observations of air quality stations for the cells in ALC and BGA may be due to the pervasive emissions in the near-source cells and therefore emissions strength better fits measurements. Differences in the O_3 concentrations between model and measurements are higher in the domain of VIC. This may be due because the photochemical O_3 production is subdued in background cells, being most of the O_3 transported from the BGA-departing plume; and hence the relative contribution from the different emissions is not as significant as in the urban or industrial cells. Despite these differences, the link between NO_x-VOC sensitivity and photochemical indicators is largely unaffected by changes in model assumptions, including assumed emission rates for both anthropogenic and biogenic species [*Sillman et al.*, 1998].

4.2. Use of Photochemical Indicators

4.2.1. NO_y

[26] NO_y works as an indicator because it is related to the balance between VOC and NO_x seen by an air mass. In addition, the association of ozone sensitivity with NO_y reflects a feature of photochemical evolution that is independent of initial VOC/NO_x ratios [*Milford et al.*, 1994]. Figure 6 shows reductions in peak O_3 associated with 35% reductions in anthropogenic VOC and NO_x emissions, plotted against the base case NO_y concentration predicted for the grid cells at 1200 UTC. Reductions in VOC have little impact on peak O_3 in locations where NO_y is low, but as NO_y increases, the reduction in O_3 associated with reduced VOC increases in an approximately log linear way. In all cases, a crossover occurs at 4 ppb NO_y, where reductions in VOC become more effective than reductions in NO_x. For the BGA and ALC scenarios, Figures 6a and 6c show a sharp delineation between VOC-sensitive (corresponding to NO_y concentrations above 4 ppb) and NO_x-sensitive locations (concentrations under this threshold). The overlap between NO_x- and VOC-sensitive locations occupies a very narrow range. Reductions of VOC in ALC yields higher O_3 reductions than in BGA. Nevertheless, results from VIC scenario (Figure 6b) illustrate a less successful correlation between sensitivity and NO_y. Here, the range of NO_y values associated with the transition regime is wider (Table 3). The difference in NO_x-VOC sensitivity between this background scenario and the urban and industrial scenarios is reflected by higher NO_y in the latter, despite NO_x- and VOC-sensitive photochemistry occurs virtually at the same NO_y in each.

4.2.2. NO_z

[27] NO_z, representing the sum of NO_x reaction products (NO_y-NO_x), can also be used as an indicator for sensitivity. Generally, NO_z has a worse correlation with sensitivity than NO_y with a broader overlap between both regimes [*Sillman*, 1995]. The indicators based on NO_y ratios can all be used for NO_z, and vice versa. Results for O_3/NO_z indicator are shown in Figure 7. For BGA and ALC (Figures 7a and 7c), the performance of O_3/NO_z as an indicator is comparable to NO_y with a well-defined transition between NO_x-sensitive chemistry ($O_3/NO_z > 22$) and VOC-sensitive chemistry (indicator values under 18). For VIC scenario (Figure 7b), this indicator performs much worse, as reflected in Table 3. Transition regime is also achieved around $O_3/NO_z \approx 20$, but the overlapping of regimes is wider, as derived from simulations. Therefore results show a strong contrast in the performance of the indicator when evaluating sensitivity regimes between different scenarios.

4.2.3. HCHO and NO_y

[28] An interesting feature of HCHO/NO_y as an indicator is that this correlation represents the impact of changes in VOC emissions. The ratio HCHO/NO_y functions as a reactivity-weighted VOC/NO_x ratio, since production of HCHO is roughly proportional to the summed rate of reactions of VOC with OH. Therefore the ratio HCHO/NO_y can also be associated with NO_x-VOC sensitivity through the analysis of odd hydrogen. Low HCHO/NO_y is associated with VOC-sensitive ozone, a result that parallels the relation between ozone sensitivity and VOC/NO_x [*Sillman and He*, 2002]. The correlation between sensitivity and HCHO/NO_y is comparable with NO_y in its consistency, although its usefulness is partially compromised by its relatively narrow range of

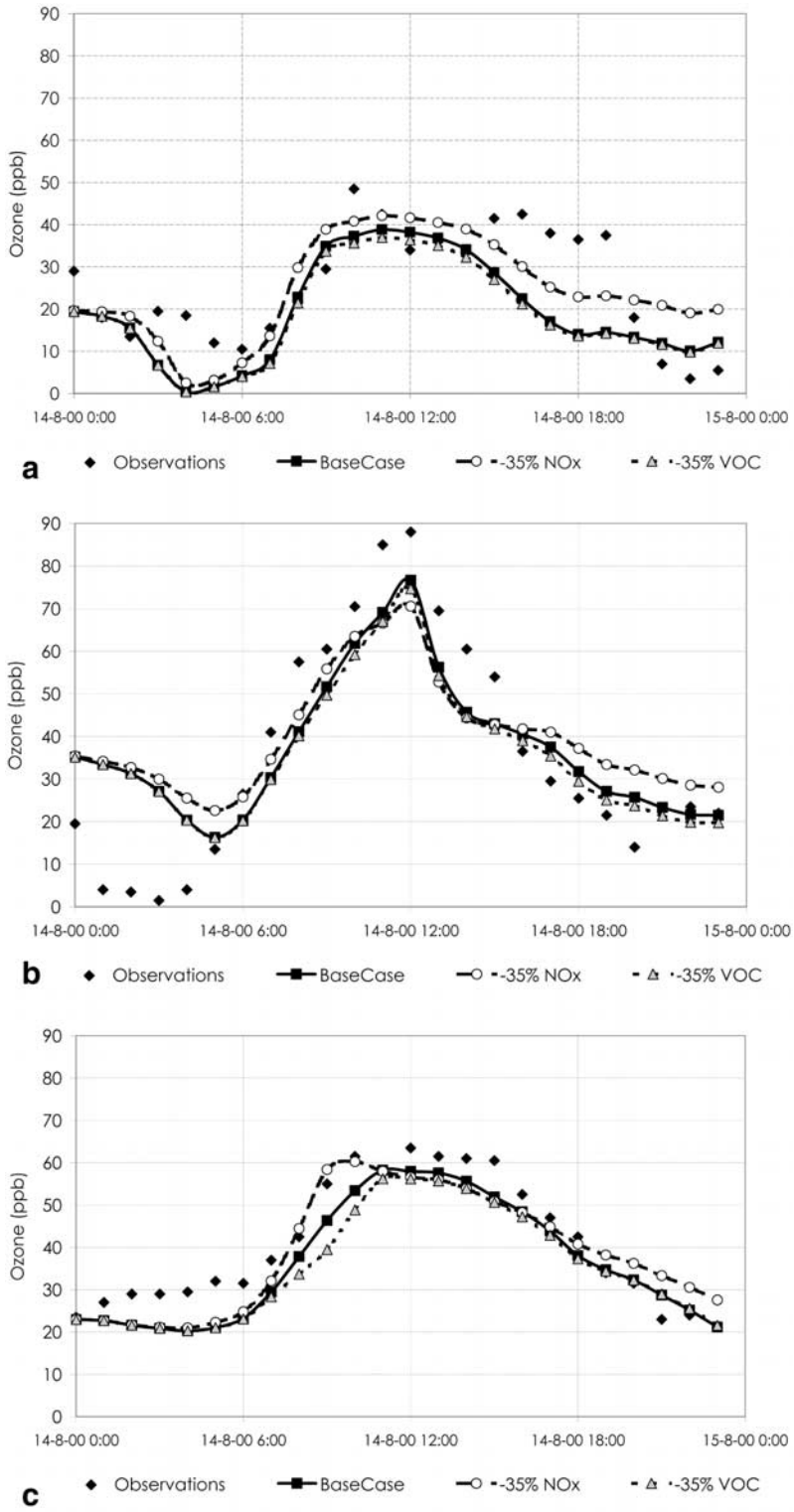

Figure 5. (a) Measured O_3 (diamonds) versus modeled O_3 for 14 August 2000 for the base case (solid line, squares), 35% NO_x reduction case (dashed line, circles), and the 35% VOC reduction case (dashed line, triangles) in stations of Barcelona (BGA). Statistical parameters are shown in Table 2. (b) Measured O_3 (diamonds) versus modeled O_3 for 14 August 2000 for the base case (solid line, squares), 35% NO_x reduction case (dashed line, circles), and the 35% VOC reduction case (dashed line, triangles) in stations of Vic. Statistical parameters are shown in Table 2. (c) Measured O_3 (diamonds) versus modeled O_3 for 14 August 2000 for the base case (solid line, squares), 35% NO_x reduction case (dashed line, circles) and the 35% VOC reduction case (dashed line, triangles) in stations of Alcover. Statistical parameters are shown in Table 2.

Table 2. Evaluation of Ozone Concentrations for 14 August 2000 According to the Scenario[a]

	Base Case	−35% NO_x	−35% VOC
Barcelona Geographical Area (Urban)			
Maximum measured, ppb	49	49	49
Maximum simulated, ppb	42	45	40
MNBE, %	−17.31	−10.16	−19.36
MNGE, %	24.11	23.76	28.16
UPA, %	−13.56	−7.94	−17.52
Plana de Vic (Background)			
Maximum measured, ppb	88	88	88
Maximum simulated, ppb	77	71	75
MNBE, %	−18.64	−19.69	−22.02
MNGE, %	27.62	31.16	28.39
UPA, %	−12.90	−19.84	−15.14
Alcover (Industrial)			
Maximum measured, ppb	64	64	64
Maximum simulated, ppb	58	60	56
MNBE, %	−14.07	−11.75	−15.68
MNGE, %	19.58	19.31	20.20
UPA, %	−8.31	−5.12	−11.47

[a]MNBE, mean normalized bias error; MNGE, mean normalized gross error; UPA, unpaired peak accuracy.

values. The model predicts the crossover between NO_x- and VOC-sensitive ozone occurs at $HCHO/NO_y \approx 0.6-0.7$ for all domains (Figure 8). Results illustrate the differences between largely NO_x-sensitive chemistry in Plana de Vic scenario and VOC sensitivity chemistry in Barcelona Geographical Area and Alcover. Nevertheless, large fractions of the model domains are associated with overlap between NO_x- and VOC- sensitive ranges (Table 3).

4.2.4. H_2O_2 and HNO_3

[29] Representation of H_2O_2 and HNO_3 chemistry involves many complex reactions and possible unknowns that become very important under low NO_x/VOC ratios [*Kuhn et al.*, 1998]. The connection between NO_x-VOC sensitivity and the ratio H_2O_2/HNO_3 is strong in the scenarios simulated. Nevertheless, this ratio behaves as an average indicator bearing in mind the overlap between NO_x- and VOC-sensitive regimes. This transition (Figure 9) takes place at a value of H_2O_2/HNO_3 of approximately 2.5–3 for the scenarios considered, being an accurate indicator in BGA and ALC (Table 3). H_2O_2/NO_y indicator is also included in Table 3, showing a similar pattern, with transition values around 0.5. For H_2O_2/NO_z, its behavior strongly depends on the domain of study, being the transition value around 0.8. The lack of a relationship between H_2O_2 and HNO_3 is partially explained by their tendency to assume different correlative patterns in NO_x- versus VOC-sensitive conditions. There is no consistent correlation between the simulated H_2O_2 and HCHO or between H_2O_2 and O_3. However, there is a triple correlation among O_3, H_2O_2 and NO_x reaction products. The sum $H_2O_2 + NO_z$ represents the cumulative sink for odd hydrogen and may be expected to correlate with O_3. As depicted in Figure 10, a correlation of this type is observed in all domains; the same type of relationship is observed for NO_z and HNO_3. This view, presented by *Sillman* [1995], emphasizes O_3 as a source for odd hydrogen, either directly or through association with intermediate hydrocarbons, and rates of formation for both peroxides and reactive nitrogen as limited by size of the odd hydrogen source. The transition from NO_x- to VOC-sensitive chemistry is linked with the replacement of peroxides by HNO_3 as the dominant sink for odd hydrogen, and therefore by a decreasing ratio of O_3 to reactive nitrogen.

4.2.5. Extent of Reaction

[30] The definition of extent of reaction [*Blanchard et al.*, 1999; *Blanchard and Stoeckenius*, 2001] used in this work has been modified in order be expressed as a function on NO_x and NO_y (equation (3)):

$$\text{Extent} = \left[1 - \frac{NO_x}{1.3 \cdot NO_y}\right] \cdot 0.67 \tag{3}$$

[31] The predicted O_3 response versus EOR exhibit considerable variability and a range of indeterminate values (0.4–0.6); nevertheless, the delimitation of the transition between NO_x and VOC limitation is fairly sharp. This parameter is correlated with NO_x-VOC sensitivity. BGA is related with the lowest values of the noon EOR (under 0.35); ALC presents EOR values between 0.35 and 0.5, corresponding to primarily VOC-sensitive sites. Meanwhile VIC (where most cells are NO_x-sensitive) presents values of EOR over 0.55.

4.2.6. NO_x-VOC Parameter

[32] It is also possible to develop a statistical correlation between NO_x-VOC sensitivity and model indicator values if a single numerical value is used to express model NO_x-VOC sensitivity. We will use the NO_x-VOC parameter (equation (4)) defined by *Sillman et al.* [1997]:

$$NO_x - \text{VOC parameter} = \frac{[O_3]_N - [O_3]_V}{\max\{[O_3]_0; [O_3]_N; [O_3]_V\} - \min\{[O_3]_0; [O_3]_N; [O_3]_V\}} \tag{4}$$

where $[O_3]_0$ represents O_3 at the specified time and location in the base case scenario, $[O_3]_N$ represents O_3 in the simulation with reduced NO_x and $[O_3]_V$ represents O_3 in the simulation with reduced VOC. The parameter is positive whenever O_3 is lower in the reduced VOC simulation than in the reduced NO_x simulation. When the O_3 reduction associated with reduced VOC is twice as large as the O_3 reduction for reduced NO_x, the parameter is 0.5; and when model NO_x reductions result in either no change or an

Figure 6. (a) Predicted reduction in peak O_3 (in ppb) resulting from a 35% reduction in the emission rate for NO_x (diamonds) and VOC (squares) plotted against NO_y (ppb) in the simulation for Barcelona geographical area. (b) Predicted reduction in peak O_3 (in ppb) resulting from a 35% reduction in the emission rate for NO_x (diamonds) and VOC (squares) plotted against NO_y (ppb) in the simulation for Plana de Vic. (c) Predicted reduction in peak O_3 (in ppb) resulting from a 35% reduction in the emission rate for NO_x (diamonds) and VOC (squares) plotted against NO_y (ppb) in the simulation for Alcover (1200 UTC).

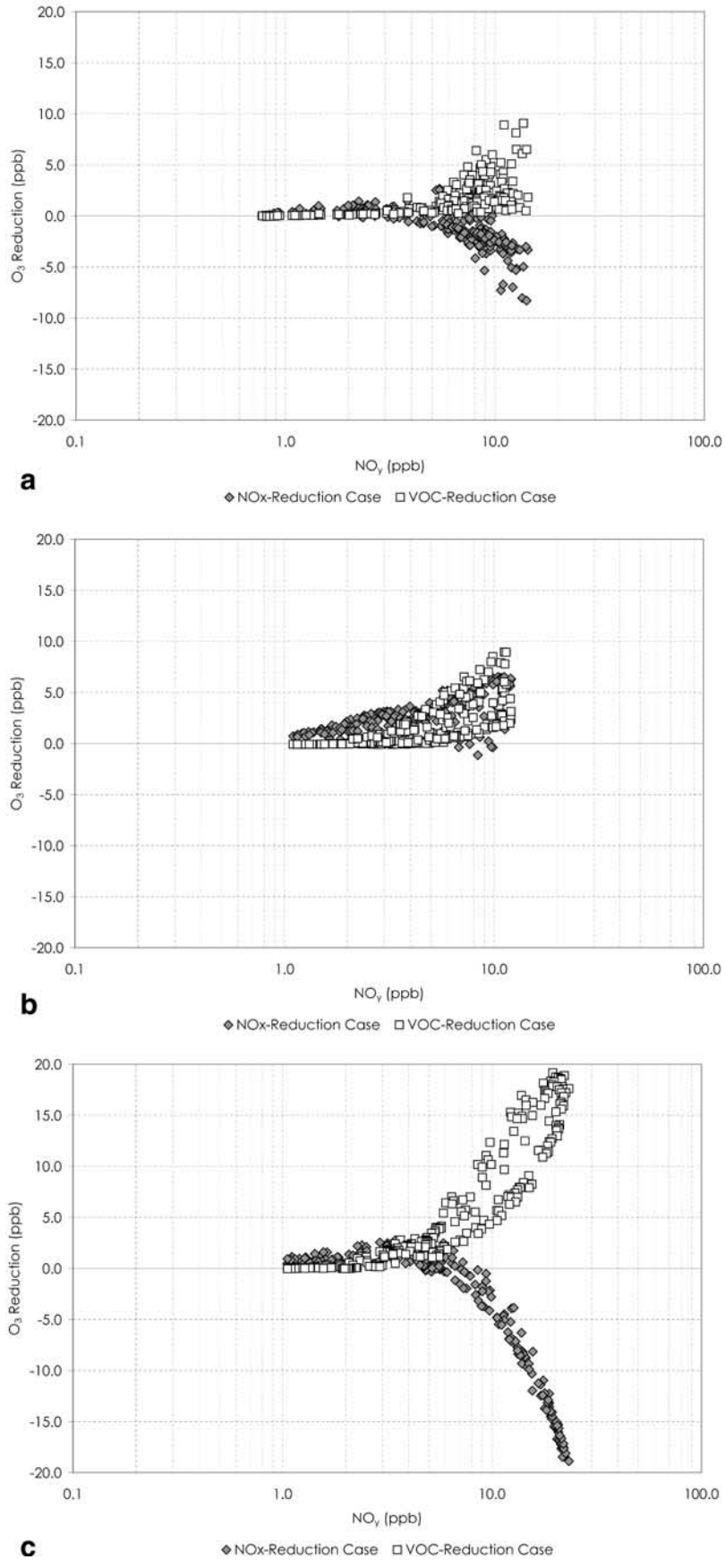
20.0
15.0
10.0
5.0
0.0
-5.0
-10.0
-15.0
-20.0
O3 Reduction (ppb)
0.1
1.0
10.0
100.0
NOy (ppb)
a
NOx-Reduction Case
VOC-Reduction Case
b
c

Figure 6

Table 3. Distribution of Photochemical Indicator Values for NO_x- and VOC-Sensitive Chemistry

	NO_x-Sensitive Locations				VOC-Sensitive Locations					
Indicator	Range	2nd Percentile	50th Percentile	98th Percentile	Range	2nd Percentile	50th Percentile	98th Percentile	Uncertainty	Correlation r^2
NO_y, ppb										
Barcelona Area	5.24–6.60	5.26	5.44	6.60	5.95–14.16	6.08	9.06	13.68	0.07	0.73
Plana de Vic	1.98–12.06	2.37	5.74	11.69	3.83–12.06	4.34	7.66	12.02	0.41	0.53
Alcover	2.28–5.86	2.31	3.18	5.42	3.45–23.33	3.93	12.19	22.05	0.22	0.71
NO_z, ppb										
Barcelona Area	3.67–4.17	3.68	3.78	4.17	1.88–6.72	2.00	3.17	6.61	0.05	0.32
Plana de Vic	1.69–9.68	1.88	5.15	9.55	2.65–9.68	3.00	6.35	9.60	0.49	0.40
Alcover	1.94–4.18	1.95	2.53	3.91	2.21–9.07	2.41	6.31	8.90	0.28	0.80
$HCHO/NO_y$										
Barcelona Area	0.34–0.38	0.34	0.37	0.38	0.18–0.53	0.20	0.31	0.51	0.09	0.78
Plana de Vic	0.28–0.87	0.32	0.45	0.77	0.33–0.60	0.34	0.42	0.55	0.52	0.40
Alcover	0.77–1.16	0.78	0.93	1.14	0.25–0.99	0.28	0.50	0.84	0.23	0.50
H_2O_2/NO_z										
Barcelona Area	0.76–0.91	0.76	0.86	0.91	0.39–2.03	0.40	1.09	1.95	0.05	0.55
Plana de Vic	0.30–2.03	0.32	0.64	1.81	0.30–1.28	0.31	0.48	1.09	0.47	0.44
Alcover	0.74–1.75	0.82	1.28	1.74	0.33–1.54	0.34	0.47	1.38	0.25	0.87
H_2O_2/NO_y										
Barcelona Area	0.48–0.64	0.48	0.57	0.64	0.19–0.60	0.19	0.38	0.59	0.18	0.75
Plana de Vic	0.24–1.74	0.27	0.57	1.51	0.24–0.88	0.24	0.40	0.76	0.41	0.50
Alcover	0.53–1.49	0.59	1.03	1.47	0.13–0.95	0.14	0.24	0.83	0.25	0.91
O_3/NO_z										
Barcelona Area	13.99–15.36	13.99	14.88	15.33	9.14–22.94	9.15	15.87	22.25	0.04	0.60
Plana de Vic	8.16–28.99	8.26	12.32	26.48	8.16–19.43	8.21	10.63	17.03	0.50	0.41
Alcover	13.93–23.64	14.59	19.43	23.64	7.08–21.20	7.16	8.93	20.04	0.27	0.87
O_3/NO_y										
Barcelona Area	8.85–10.76	8.85	10.45	10.73	3.13–9.17	3.47	5.64	8.15	0.02	0.75
Plana de Vic	6.45–24.84	6.57	10.79	21.59	6.35–13.43	6.54	8.83	12.51	0.38	0.50
Alcover	9.92–20.14	10.56	15.41	19.95	2.72–14.73	2.77	4.84	12.81	0.12	0.93
O_3/HNO_3										
Barcelona Area	17.29–18.75	17.29	18.09	18.73	10.70–32.09	11.14	20.88	30.84	0.04	0.57
Plana de Vic	11.72–49.40	11.93	17.18	44.33	11.72–26.39	11.78	15.27	23.20	0.59	0.39
Alcover	20.31–36.07	20.99	27.99	35.92	8.49–27.64	8.70	11.09	26.93	0.22	0.84
H_2O_2/HNO_3										
Barcelona Area	0.94–1.12	0.94	1.05	1.11	0.49–2.75	0.50	1.49	2.61	0.04	0.50
Plana de Vic	0.44–3.45	0.47	0.89	3.04	0.44–1.74	0.45	0.69	1.45	0.57	0.41
Alcover	1.08–2.66	1.17	1.84	2.65	0.42–1.92	0.43	0.56	1.80	0.18	0.85
EOR										
Barcelona Area	0.48–0.53	0.48	0.51	0.52	0.24–0.54	0.24	0.36	0.50	0.07	0.80
Plana de Vic	0.50–0.65	0.51	0.60	0.64	0.39–0.63	0.43	0.57	0.63	0.63	0.57
Alcover	0.48–0.59	0.49	0.56	0.59	0.35–0.58	0.35	0.42	0.54	0.30	0.77

increase in O_3, the parameter is 1. Negative values represent equivalent NO_x-sensitive results. The quality of the NO_x-VOC indicator correlation is demonstrated by three factors [*Sillman et al.*, 1997]: (1) the size of the difference between indicator values associated with NO_x-sensitive, VOC-sensitive and transitional chemistry; (2) the lack of overlap between indicator values associated with NO_x- and VOC-sensitive locations; and (3) the consistency of the NO_x-VOC transition value in different simulations. As seen in Table 3 and Figure 11, this parameter correlates with model values for most photochemical indicators. Correlation coefficients (r^2) of 0.50 or higher are found for all simulations and indicators. Correlation is lower for Plana de Vic since most of the domain is strongly NO_x-sensitive, and the wide range of indicator values among NO_x-sensitive locations lowers the statistical correlation.

4.3. Uncertainties

[33] The use of base model chemical relationship involves uncertainties based on model simplifications [*Jiménez et al.*, 2003]. We define the uncertainty of the indicators as the fraction of the model domain with indicator values that are within 20% of the range of indicator values associated with the opposite NO_x-VOC sensitivity. This parameter is recorded for each indicator and each domain in Table 3 and will help identifying

Figure 7. (a) Predicted reduction in peak O_3 (in ppb) resulting from a 35% reduction in the emission rate for NO_x (diamonds) and VOC (squares) plotted against O_3/NO_z in the simulation for Barcelona geographical area. (b) Predicted reduction in peak O_3 (in ppb) resulting from a 35% reduction in the emission rate for NO_x (diamonds) and VOC (squares) plotted against O_3/NO_z in the simulation for Plana de Vic. (c) Predicted reduction in peak O_3 (in ppb) resulting from a 35% reduction in the emission rate for NO_x (diamonds) and VOC (squares) plotted against O_3/NO_z in the simulation for Alcover (1200 UTC).

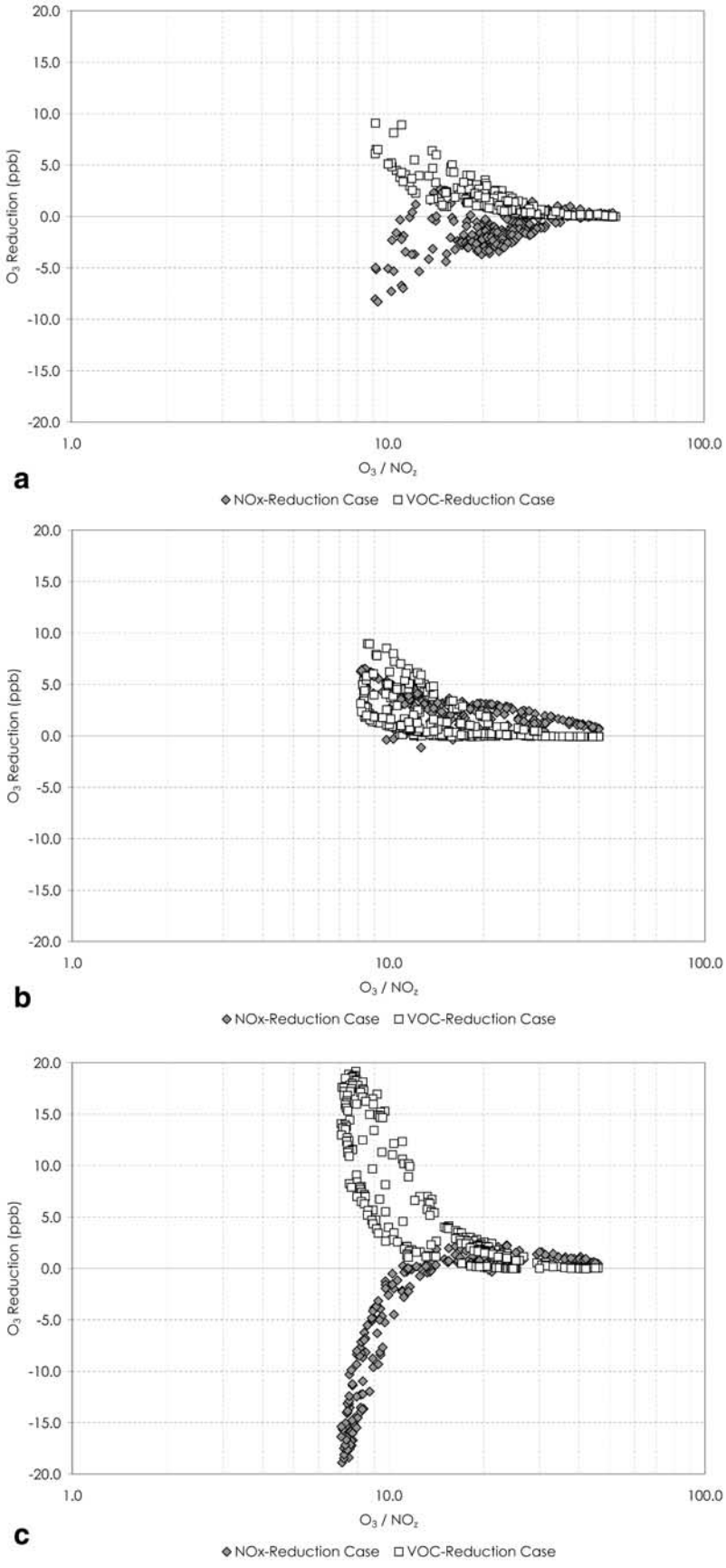
20.0
15.0
10.0
5.0
0.0
-5.0
-10.0
-15.0
-20.0
O3 Reduction (ppb)
1.0
10.0
100.0
O3 / NOz
a
NOx-Reduction Case
VOC-Reduction Case
b
c

Figure 7

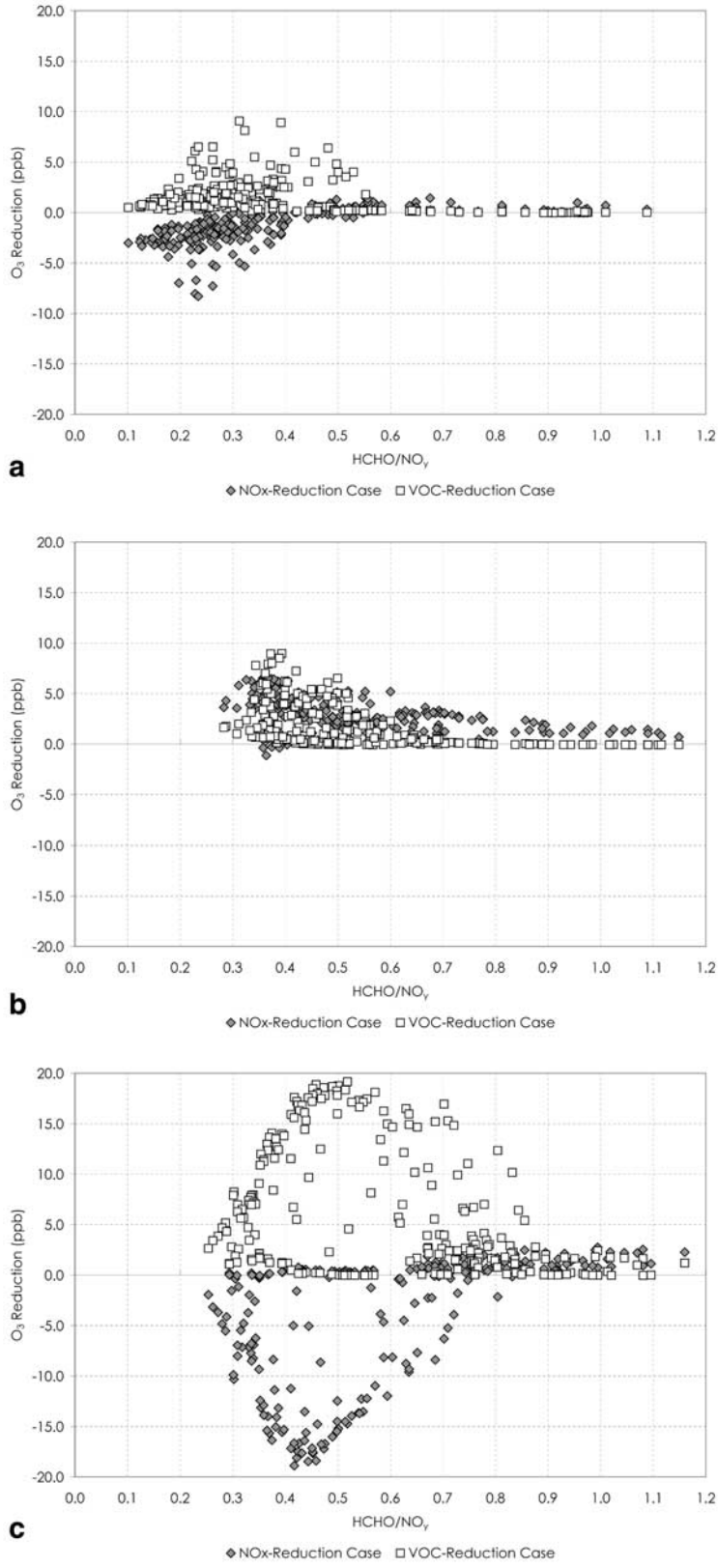

Figure 8. (a) Predicted reduction in peak O_3 (in ppb) resulting from a 35% reduction in the emission rate for NO_x (diamonds) and VOC (squares) plotted against $HCHO/NO_y$ in the simulation for Barcelona geographical area. (b) Predicted reduction in peak O_3 (in ppb) resulting from a 35% reduction in the emission rate for NO_x (diamonds) and VOC (squares) plotted against $HCHO/NO_y$ in the simulation for Plana de Vic. (c) Predicted reduction in peak O_3 (in ppb) resulting from a 35% reduction in the emission rate for NO_x (diamonds) and VOC (squares) plotted against $HCHO/NO_y$ in the simulation for Alcover (1200 UTC).

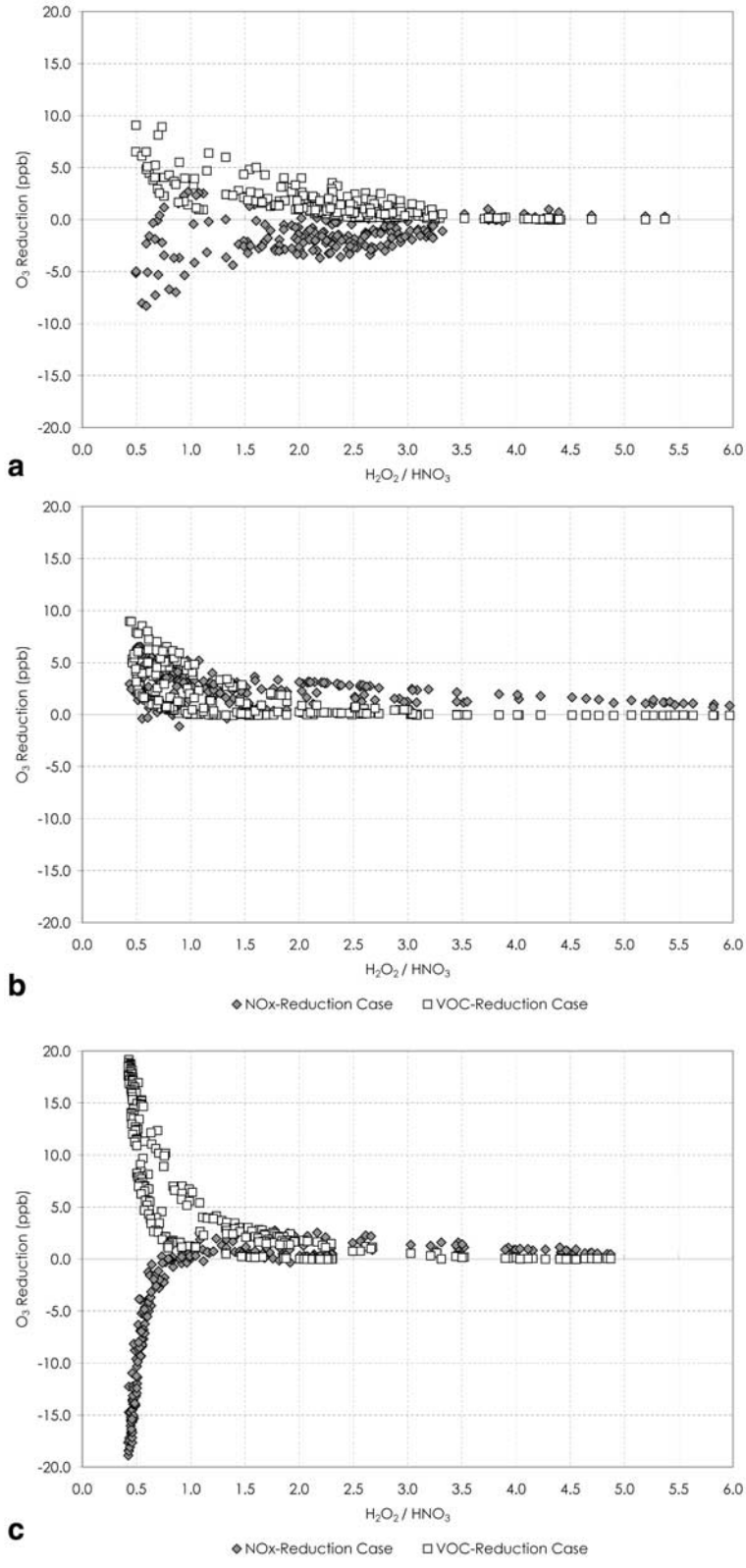

Figure 9. (a) Predicted reduction in peak O_3 (in ppb) resulting from a 35% reduction in the emission rate for NO_x (diamonds) and VOC (squares) plotted against H_2O_2/HNO_3 in the simulation for Barcelona geographical area. (b) Predicted reduction in peak O_3 (in ppb) resulting from a 35% reduction in the emission rate for NO_x (diamonds) and VOC (squares) plotted against H_2O_2/HNO_3 in the simulation for Plana de Vic. (c) Predicted reduction in peak O_3 (in ppb) resulting from a 35% reduction in the emission rate for NO_x (diamonds) and VOC (squares) plotted against H_2O_2/HNO_3 in the simulation for Alcover (1200 UTC).

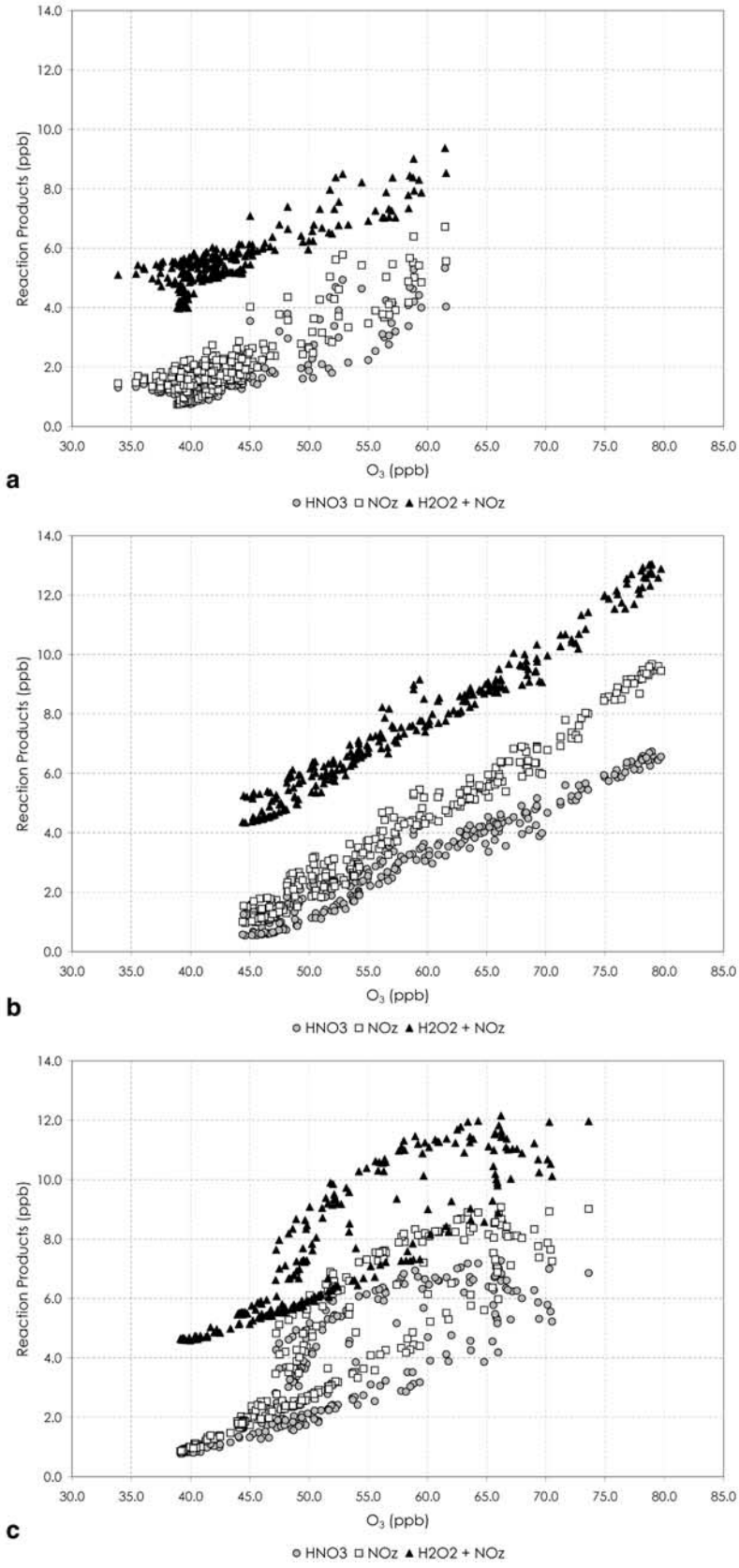

Figure 10. (a) HNO_3 (circles), NO_z (squares), and H_2O_2 + NO_z (triangles) versus O_3, all in ppb, at 1200 UTC in simulations for Barcelona geographical area. (b) HNO_3 (circles), NO_z (squares), and H_2O_2 + NO_z (triangles) versus O_3, all in ppb, at 1200 UTC in simulations for Plana de Vic. (c) HNO_3 (circles), NO_z (squares), and H_2O_2 + NO_z (triangles) versus O_3, all in ppb, at 1200 UTC in simulations for Alcover.

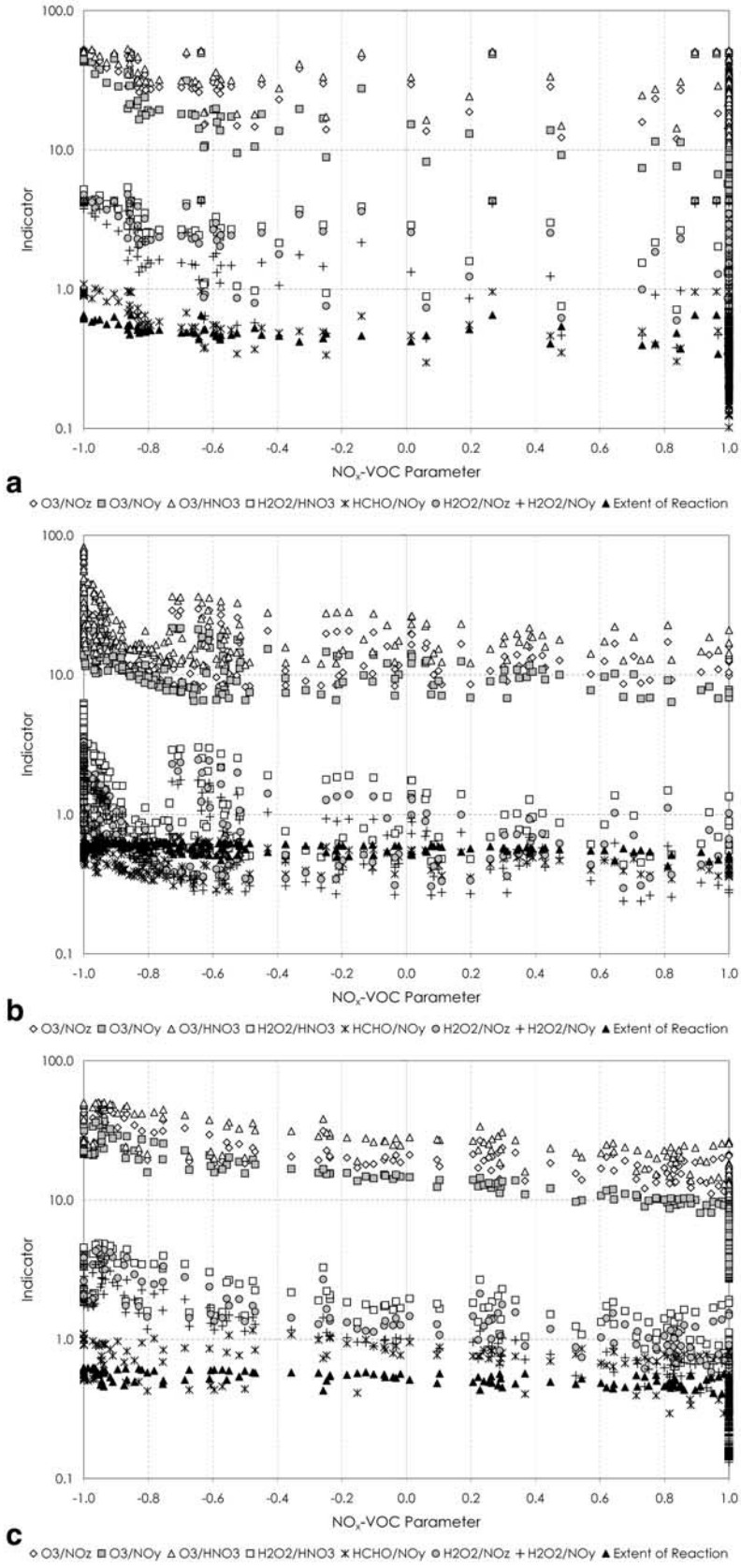

Figure 11. (a) Indicators versus NO_x-VOC parameter at 1200 UTC in simulations for Barcelona Geographical Area. (b) Indicators versus NO_x-VOC parameter at 1200 UTC in simulations for Plana de Vic. (c) Indicators versus NO_x-VOC parameter at 1200 UTC in simulations for Alcover.

their usefulness. The extent of overlap between NO_x-sensitive and VOC-sensitive ranges for indicator species and model domains provides a partial representation of the uncertainties associated with the sensitivity indicator correlations. The uncertainty factor is relatively higher for every indicator involving H_2O_2 and HNO_3, especially in VIC, which is mainly a NO_x-limited scenario, since of the high solubilities of these species, which makes them sensitive to surface deposition and aerosol formation rates (as stated by *Sillman* [1995]), which involve vague representation in photochemical models. H_2O_2 is vulnerable to reaction rate and mechanism uncertainties, so it must be considered carefully when using it as an indicator of sensitivity regime. Smallest uncertainties are achieved when using indicators related to total reactive nitrogen (NO_y or O_3/NO_y), in the order of 5% for BGA, 40% for VIC and 10% for ALC. NO_z-related indicators (NO_z, O_3/NO_z, H_2O_2/NO_z) carry a high uncertainty when used in VIC domain (NO_x-limited); nevertheless, its uncertainty decreases in VOC-limited domains as BGA or ALC. NO_z is expected to vary significantly in response to changes in radiation and production rates of odd hydrogen. The uncertainty in the relationship between extent of reaction and NO_x- or VOC-sensitive regimes is also low, since transition range is well delimited; in addition, it exhibits a good correlation with the NO_x-VOC parameter as previously defined.

[34] Table 3 presents a summary of transition regimes for all indicators, as well as 2nd, 50th and 98th percentiles of indicators in NO_x- and VOC-sensitive locations for both scenarios. Results show that median values for indicators involving NO_y or NO_z species diverge in a factor of approximately 2–3 in the scenario of BGA and VIC; on the other side, no relevant difference is shown for this indicators in VIC, a domain whose cells are mainly NO_x-limited. For O_3/HNO_3 and H_2O_2/HNO_3, NO_x-sensitive locations exhibit a higher value than VOC-sensitive locations in both domains by a factor of 2. The 98th percentile of the distribution of indicator values for NO_x-sensitive locations is approximately equal than the 2nd percentile of the indicator distribution for VOC-sensitive locations in the case of NO_y, NO_z, demonstrating the robustness of the correlation between indicator values and NO_x-VOC sensitivity. Other indicators that permit us establish an accurate transition regime independently of the domain considered are $HCHO/NO_y$, O_3/NO_y, H_2O_2/HNO_3 and extent of reaction, where the 98th percentile VOC-sensitive value is of the same magnitude than the 2nd percentile NO_x-sensitive value.

5. Conclusions

[35] This study has provided a case study of how the method of photochemical indicators can be used to evaluate O_3-NO_x-VOC sensitivity in very complex terrains, showing the correlation between photochemical indicators and simulated NO_x-VOC sensitivity in a terrain as complex as the northeastern Iberian Peninsula during a typical recirculation episode of photochemical pollution. The model evaluation shown here is relatively simple to perform and provides a test for sensitivity evaluation and to establish control policies for ozone precursor emissions. Nevertheless, indicators are subject to many uncertainties, including deposition rates, aerosol interactions and case-to-case variations.

[36] Results shown suggest that O_3 chemistry in the Barcelona city plume arriving at VIC is close to the transition between VOC-sensitive and NO_x-sensitive conditions. Nevertheless, BGA and ALC present a high VOC-sensitive behavior due to the high traffic and industrial NO_x emissions. Predicted NO_x-VOC sensitivity varies considerably among the three model scenarios. NO_x-sensitive chemistry is associated with lower O_3 and NO_y; the varying NO_x-VOC predictions occur despite O_3 is similar in all three scenarios.

[37] Variations in indicator behavior are analytically linked to variations in the O_3 production efficiency per primary radical production. In general, H_2O_2- and HNO_3-derived indicators entail higher uncertainties since transition regimes between NO_x and VOC sensitivity cover a wide range, because those indicators (and their ratio) is affected by changes in environmental conditions. NO_y and O_3/NO_y are revealed as the most accurate indicators to assess sensitivity in the domains studied, attending to the narrow transition regime between NO_x- and VOC-sensitive chemistry and the low uncertainty observed; on the other side, NO_z indicators correlates worse than NO_y and implies a higher uncertainty. The behavior of NO_z tends to disagree for differently polluted domains; hence it performs better in VOC-sensitive (BGA, a metropolitan area; or ALC, an industrial zone characterized by high NO_x and VOC emissions) than in NO_x-sensitive scenarios as VIC. The extent of reaction also performs as a good indicator to separate NO_x and VOC sensitive regimes. The results given in this study indicate the necessity to consider the differences in the conditions of the domains when applying the indicator approach.

[38] The biggest weakness of these indicators is the difficulty in testing the predicted indicator-NO_x-VOC relationship against ambient measurements. In addition, the indicator method provides information about NO_x-VOC sensitivity at the time and place considered. NO_x-VOC sensitivity varies with time of day, changes from event to event, and by location within a same domain.

[39] **Acknowledgments.** This work was developed under the research contract REN2003-09753-C02 of the Spanish Ministry of Science and Technology. The Spanish Ministry of Education is also thanked for the FPU doctoral fellowship hold by P. Jiménez. Meteorological and air quality stations data are provided by the Environmental Department of the Catalonia Government. The authors gratefully acknowledge O. Jorba, R. Parra and A. Stein for the helpful discussions.

References

Andreani-Aksoyoglu, S., C.-H. Lu, J. Keller, A. S. H. Prévôt, and J. S. Chang (2001), Variability of indicator values for ozone production sensitivity: A model study in Switzerland and San Joaquin Valley (California), *Atmos. Environ.*, *35*, 5593–5604.

Atkinson, R. (2000), Atmospheric chemistry of VOCs and NO_x, *Atmos. Environ.*, *34*, 2063–2101.

Baldasano, J. M., L. Cremades, and C. Soriano (1994), Circulation of air pollutants over the Barcelona geographical area in summer, in *Proceedings of the 6th European Symposium on Physico-Chemical Behaviour of Atmospheric Pollutants. Varese (Italy)*, *Rep. EUR 15609/1 EN*, pp. 474–479, Eur. Comm., Brussels.

Barros, N., I. Toll, C. Soriano, P. Jiménez, C. Borrego, and J. M. Baldasano (2003), Urban photochemical pollution in the Iberian peninsula: The Lisbon and Barcelona airsheds, *J. Air Waste Manage. Assoc.*, *53*, 347–359.

Blanchard, C. L., and D. Fairley (2001), Spatial mapping of VOC and NO_x-limitation of ozone formation in central California, *Atmos. Environ.*, *35*, 3861–3873.

Blanchard, C. L., and T. Stoeckenius (2001), Ozone response to precursor controls: Comparison of analysis methods with the predictions of photochemical air quality simulation models, *Atmos. Environ.*, *35*, 1203–1215.

Blanchard, C. L., F. W. Lurmann, P. M. Roth, H. E. Jeffries, and M. Korc (1999), The use of ambient data to corroborate analyses of ozone control strategies, *Atmos. Environ.*, *33*, 369–381.

Byun, D. W., and J. K. S. Ching (Eds.) (1999), Science algorithms of the EPA Models-3 Community Multiscale Air Quality (CMAQ) Modeling System, *Rep. N. EPA-600/R-99/030*, Off. of Res. and Dev., U.S. Environ. Prot. Agency, Washington, D. C.

Gery, M. W., G. Z. Whitten, J. P. Killus, and M. C. Dodge (1989), A photochemical kinetics mechanism for urban and regional scale computer modeling, *J. Geophys. Res.*, *94*, 12,925–12,956.

Hogrefe, C., S. T. Rao, P. Kasibhatla, W. Hao, G. Sistla, R. Mathur, and J. McHenry (2001), Evaluating the performance of regional-scale photochemical modeling systems: Part II—Ozone predictions, *Atmos. Environ.*, *35*, 4175–4188.

Huang, H.-C., and J. S. Chang (2001), On the performance of numerical solvers for a chemistry submodel in three-dimensional air quality models, *J. Geophys. Res.*, *106*, 20,175–20,188.

Jiménez, P., D. Dabdub, and J. M. Baldasano (2003), Comparison of photochemical mechanisms for air quality modeling, *Atmos. Environ.*, *37*, 4179–4194.

Jorba, O., C. Pérez, F. Rocadenbosch, and J. M. Baldasano (2004), Cluster analysis of 4-day back trajectories arriving in the Barcelona area (Spain) from 1997 to 2002, *J. Appl. Meteorol.*, *43*(6), 887–901.

Kleinman, L. I., P. H. Daum, J. H. Lee, Y.-N. Lee, L. J. Nunnermacjerm, S. R. Springston, L. Newman, J. Weinstein-Lloyd, and S. Sillman (1997), Dependence of ozone production on NOx and hydrocarbons in the troposphere, *Geophys. Res. Lett.*, *24*, 2299–2302.

Kuhn, M., et al. (1998), Intercomparison of the gas-phase chemistry in several chemistry and transport models, *Atmos. Environ.*, *32*, 693–709.

Lu, C.-H., and J. Chang (1998), On the indicator-based approach to assess ozone sensitivities and emission features, *J. Geophys. Res.*, *103*, 3453–3462.

Mesoscale and Microscale Meteorology Division (2001), PSU/NCAR mesoscale modeling system tutorial class notes and user's guide: MM5 modeling system version 3, Natl. Cent. for Atmos. Res., Boulder, Colo.

Milford, J. B., D. Gao, S. Sillman, P. Blossey, and A. G. Russell (1994), Total reactive nitrogen (NO_y) as an indicator of the sensitivity of ozone to reductions in hydrocarbon and NO_x emissions, *J. Geophys. Res.*, *99*, 3533–3542.

Millán, M., R. Salvador, E. Mantilla, and G. Kallos (1997), Photooxidant dynamics in the Mediterranean basin in summer: Results from European research projects, *J. Geophys. Res.*, *102*, 8811–8823.

Ntziachristos, L., and Z. Samaras (2000), COPERTIII computer programme to calculate emissions from road transport. Methodology and emission factors (version 2.1), *Tech. Rep. 49*, Eur. Environ. Agency, Copenhagen.

Parra, R. (2004), Development of the EMICAT2000 model for the estimation of air pollutants emissions in Catalonia and its use in photochemical dispersion models (in Spanish), Ph.D. dissertation, Polytech. Univ. of Catalonia, Barcelona, Spain.

Parra, R., and J. M. Baldasano (2004), Modelling the on-road traffic emissions from Catalonia (Spain) for photochemical air pollution research: Weekday-weekend differences, paper presented at Air Pollution 2004: Twelfth International Conference on Modelling, Monitoring and Management of Air Pollution, Wessex Inst. of Technol., Rhodes, Greece.

Parra, R., S. Gassó, and J. M. Baldasano (2004), Estimating the biogenic emissions of non-methane volatile organic compounds from the north western Mediterranean vegetation of Catalonia, Spain, *Sci. Total Environ.*, *329*, 241–259.

Pérez, C., M. Sicard, O. Jorba, A. Comerón, and J. M. Baldasano (2004), Summertime re-circulations of air pollutants over the north-eastern Iberian coast observed from systematic EARLINET lidar measurements in Barcelona, *Atmos. Environ.*, *38*, 3983–4000.

Russell, A., and R. Dennis (2000), NARSTO critical review of photochemical models and modeling, *Atmos. Environ.*, *34*, 2283–2324.

Sillman, S. (1995), The use of NO_y, H_2O_2 and HNO_3 as indicators for ozone-NO_x-hydrocarbon sensitivity in urban locations, *J. Geophys. Res.*, *100*, 14,175–14,188.

Sillman, S. (1999), The relation between ozone, NO_x and hydrocarbons in urban and polluted rural environments, *Atmos. Environ.*, *33*, 1821–1845.

Sillman, S., and D. He (2002), Some theoretical results concerning O_3-NO_x-VOC chemistry and NO_x-VOC indicators, *J. Geophys. Res.*, *107*(D22), 4659, doi:10.1029/2001JD001123.

Sillman, S., D. He, C. Cardelino, and R. E. Imhoff (1997), The use of photochemical indicators to evaluate ozone-NO_x-hydrocarbon sensitivity: Case studies from Atlanta, New York and Los Angeles, *J. Air Waste Manage. Assoc.*, *47*, 1030–1040.

Sillman, S., D. He, M. R. Pippin, P. H. Daum, D. G. Imre, L. I. Kleinman, J. H. Lee, and J. Weinstein-Lloyd (1998), Model correlations for ozone, reactive nitrogen and peroxides for Nashville in comparison with measurements: Implications for VOC-NO_x sensitivity, *J. Geophys. Res.*, *103*, 22,629–22,644.

Sillman, S., R. Vautard, L. Menut, and D. Kley (2003), O_3-NO_x-VOC sensitivity and NO_x-VOC indicators in Paris: Results from models and atmospheric pollution over the Paris area (ESQUIF) measurements, *J. Geophys. Res.*, *108*(D17), 8563, doi:10.1029/2002JD001561.

Toll, I., and J. M. Baldasano (2000), Modeling of photochemical air pollution in the Barcelona area with highly disaggregated anthropogenic and biogenic emissions, *Atmos. Environ.*, *34*(19), 3060–3084.

Tonnesen, G. S., and R. L. Dennis (2000a), Analysis of radical propagation efficiency to assess ozone sensitivity to hydrocarbons and NO_x: 1. Local indicators of instantaneous odd oxygen production sensitivity, *J. Geophys. Res.*, *105*, 9213–9226.

Tonnesen, G. S., and R. L. Dennis (2000b), Analysis of radical propagation efficiency to assess ozone sensitivity to hydrocarbons and NO_x: 2. Long-lived species as indicators of ozone concentration sensitivity, *J. Geophys. Res.*, *105*, 9227–9242.

U.S. Environmental Protection Agency (1991), Guideline for regulatory application of the urban airshed model, *Rep. EPA-450/4-91-013*, Off. of Air and Radiat., Research Triangle Park, N. C.

J. M. Baldasano and P. Jiménez, Laboratory of Environmental Modeling, Universitat Politècnica de Catalunya (UPC), Avda. Diagonal 647 10.23, E-08028 Barcelona, Spain. (jose.baldasano@upc.es)